



Contribution of peripheral blood mononuclear cells isolated by advanced filtration system to myogenesis of human bone marrow mesenchymal stem cells co-cultured with myoblasts

Pasqualina Scala^a, Paola Manzo^b, Raffaele Longo^c, Valentina Giudice^{a,b}, Maria Camilla Ciardulli^a, Bianca Serio^b, Carmine Selleri^{a,b}, Liberata Guadagno^c, Laura Rehak^d, Nicola Maffulli^{a,e}, Giovanna Della Porta^{a,f,*}

^a Department of Medicine, Surgery and Dentistry, University of Salerno, Via S. Allende, 43, 84081 Baronissi SA, Italy

^b Hematology and Transplant Center, University Hospital "San Giovanni di Dio e Ruggi D'Aragona", Largo Città d'Ippocrate, 1, 84131 Salerno SA, Italy

^c Department of Industrial Engineering, University of Salerno, Via Giovanni Paolo II, 132, 84084 Fisciano SA, Italy

^d Athena Biomedical Innovations, Viale Europa 139, Florence, 50126, Italy

^e Centre for Sports and Exercise Medicine, Barts and the London School of Medicine and Dentistry, Queen Mary University of London, 275 Bancroft Road, London E1 4DG, UK

^f Interdepartment Centre BIONAM, Università di Salerno, via Giovanni Paolo II, 132, 84084 Fisciano SA, Italy

ARTICLE INFO

Keywords:

Blood filtration
Poly-butylene terephthalate membrane
Peripheral blood mononuclear cell
Myogenesis

ABSTRACT

Background: Contribution of peripheral blood mononuclear cells (PBMCs) in myogenesis is still under debate, even though blood filtration systems are commonly used in clinical practice for successfully management of critic limb ischemia.

Objectives: A commercial blood filter used for autologous human PBMC transplantation procedures is characterized and used to collect PBMCs, that are then added to well-established 2D *in vitro* myogenic models assembled with a co-culture of human bone marrow-derived mesenchymal stem cells (hBM-MSCs) and skeletal myoblasts (hSkMs) with the aim of investigating their potential contribution to stem cell myogenic commitment.

Methods: A commercial blood filter was physically and chemically studied to understand its morphological characteristics and composition. PBMCs were concentrated using this system, further isolated by Ficoll-Paque density gradient centrifugation, and then added in an upper transwell chamber to a 2D co-culture of hBM-MSCs and hSkMs. Myogenic commitment was investigated by RT-PCR, immunofluorescence, and flow cytometry immunophenotyping. Cytokine levels were monitored by ELISA assay in culture media.

Results: The blood filtration system was disassembled and appeared to be formed by twelve membranes of poly-butylene terephthalate fibers (diameters, 0.9–4.0 μm) with pore size distribution of 1–20 μm. Filter functional characterization was achieved by characterizing collected cells by flow cytometry. Subsequently, collected PBMCs fraction was added to an *in-vitro* model of hBM-MSC myogenic commitment. In the presence of PBMCs, stem cells significantly upregulated myogenic genes, such as *Desmin* and *MYH2*, as confirmed by qRT-PCR and expressed related proteins by immunofluorescence (IF) assay, while downregulated pro-inflammatory cytokines (*IL12A* at day 14) along the 21 days of culture.

* Corresponding author. Department of Medicine, Surgery and Dentistry, University of Salerno, Via S. Allende, Baronissi SA 84084, Italy. ;
E-mail address: gdellaporta@unisa.it (G. Della Porta).

<https://doi.org/10.1016/j.heliyon.2023.e17141>

Received 3 November 2022; Received in revised form 6 June 2023; Accepted 8 June 2023

Available online 9 June 2023

2405-8440/© 2023 The Authors. Published by Elsevier Ltd. This is an open access article under the CC BY-NC-ND license (<http://creativecommons.org/licenses/by-nc-nd/4.0/>).

Novelty: Our work highlights chemical-physical properties of commercial blood filter and suggests that blood filtrated fraction of PBMC might modulate cytokine expression in response to muscle injury and promote myogenic events, supporting their clinical use in autologous transplantation.

1. Introduction

Several blood filtration systems are used in clinical practice to concentrate Peripheral Blood Mononuclear Cell (PBMC) fraction from whole blood with extremely low residual red blood cells. These systems are safe, fast, sterile, and minimally invasive procedures for autologous transplantation of blood fraction. Indeed, autologous PBMCs can promote tissue healing at the site of injury, such as during critic limb ischemia (CLI) ineligible for revascularization procedures where myofiber regeneration significantly increases and limb rescue improves [1–3]. This aspect is of particular interest as skeletal muscles have limited self-renewal ability, and healing process fails in severe injuries, like volumetric muscle loss (VML), characterized by extensive scar tissue formation, permanent loss of muscle function, and chronic inflammation [4]. Filtration systems with different composition and pore size range, as indicated in the patent no. EPO 2602315A1, are built using several types of polymers likely using melt-blowing technology, and are organized in multilayers with positively- or negatively charged surfaces influencing its hydrophilicity and its capacity to differentially retain or filter various cell types [5–7].

Conversely, reconstructive surgery using autologous tissue grafts is the main approach to VML management; however, several limitations are present, such as poor tissue availability, long-term dysfunction with loss of muscle strength, and risk of infectious complications [4]. The exact mechanism by which autologous PBMCs support both muscle and vascular healing in CLI is still unclear, as well as how PBMCs influence myogenic events, even though pharmacological targeting of inflammation and immune functions result in faster healing processes. In case of severe injuries, skeletal muscle capacity to spontaneously heal appears insufficient, and

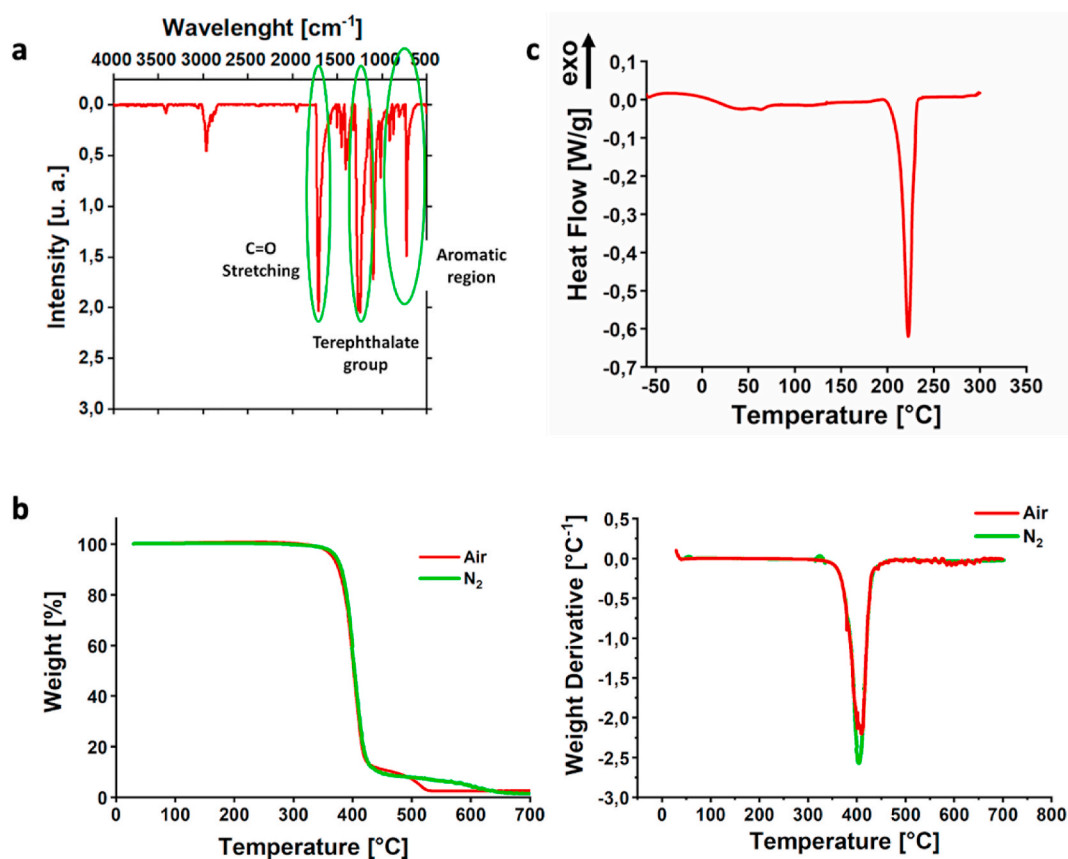


Fig. 1. Filtration system characterization: physical and chemical properties. FTIR of the commercial filter (A); DSC of the filter disk (B); TGA and DTGA of the commercial filter (C). Polybutylene terephthalate (PBT) fibers were identified in filter membranes by FTIR spectroscopy (A) by the presence of the terephthalate group, the aromatic group and the stretching of C=O of the carbonyl group evident in the FT/IR spectrum, Profiles of TGA curves evidenced membrane stability up to 350 °C both in reactive and inert environment (B), with the main degradation step occurring at around 400 °C. DSC curve showed the glass transition of materials at around 30 °C, and the melting temperature at about 223 °C (C).

available treatments do not provide optimal restoration to preinjury status [8]. Therefore, biological treatments, including cell therapy and tissue engineering protocols, are of clinical interest, and a biomimetic *in vitro* model could be a precious tool to better understand the complex mechanism behind healing processes to improve clinical management. Tissue engineering approaches include scaffolds [9], nanocarriers for drug delivery [10], and new therapeutic strategies, like cell therapy, still under investigation in case of skeletal muscle injuries. Indeed, muscle stem cells (also termed satellite cells) are the most promising sources of stem cells, although their clinical efficacy is under debate, as these cells are poorly represented in muscle tissue, are difficult to harvest by both mechanic and enzymatic degradation, and lose their engraftment potential in *ex vivo* conditions [11–13]. Other sources of stem cells are human bone marrow (*hBM*)-derived mesenchymal stem cells (MSCs) or Wharton Jelly mesenchymal stem cells (WJ-MSC), because of their broad potential to differentiate towards different phenotypes [14–20], low immunogenicity, and immunomodulatory activity [21,22]. To date, BM-MSC clinical application after severe muscle trauma are restricted to animal models where stem cells favor muscle regeneration, with successful improvement of contractile muscle force [23–25]. Autologous PBMC transplantation is another therapeutic option widely used in clinical practice for revascularization procedures, as those performed for lower limb ischemia treatments [26, 27], or for non-healing ischemic ulcers [28].

Skeletal muscle injuries also trigger inflammation [29] and innate and adaptive immune responses, as immune populations are involved in a wide range of functions, such as clearance of necrotic debris, inflammation, remodeling phase modulation [30], and release of multiple soluble factors contributing to healing process, like interferon- γ (IFN- γ) [31], tumor necrosis factor (TNF) [32], or interleukin (IL)s [33,34]. For example, IL-10, an anti-inflammatory cytokine, favors the transition from proliferative to differentiation phase of myogenesis [35,36].

In the present study, structure, morphology, and chemical composition of a commercial filter was investigated by optical and electron microscope, Fourier-transform infrared spectroscopy (FTIR), Differential Scanning Calorimetry (DSC), and Thermogravimetric analysis (TGA) analyses. Functional characterization was performed by flow cytometry immunophenotyping of filtered PBMCs. Subsequently, to better understand the role of collected PBMC in myogenic events, filtered fractions were co-cultured with a previously described *in-vitro* myogenic model using a co-culture with *hBM*-MSCs and human skeletal muscle cells (*hSkMs*) [14]. *hBM*-MSC myogenic commitment was monitored by gene expression profiling by RT-qPCR and by immunofluorescence (IF) assay. The influence

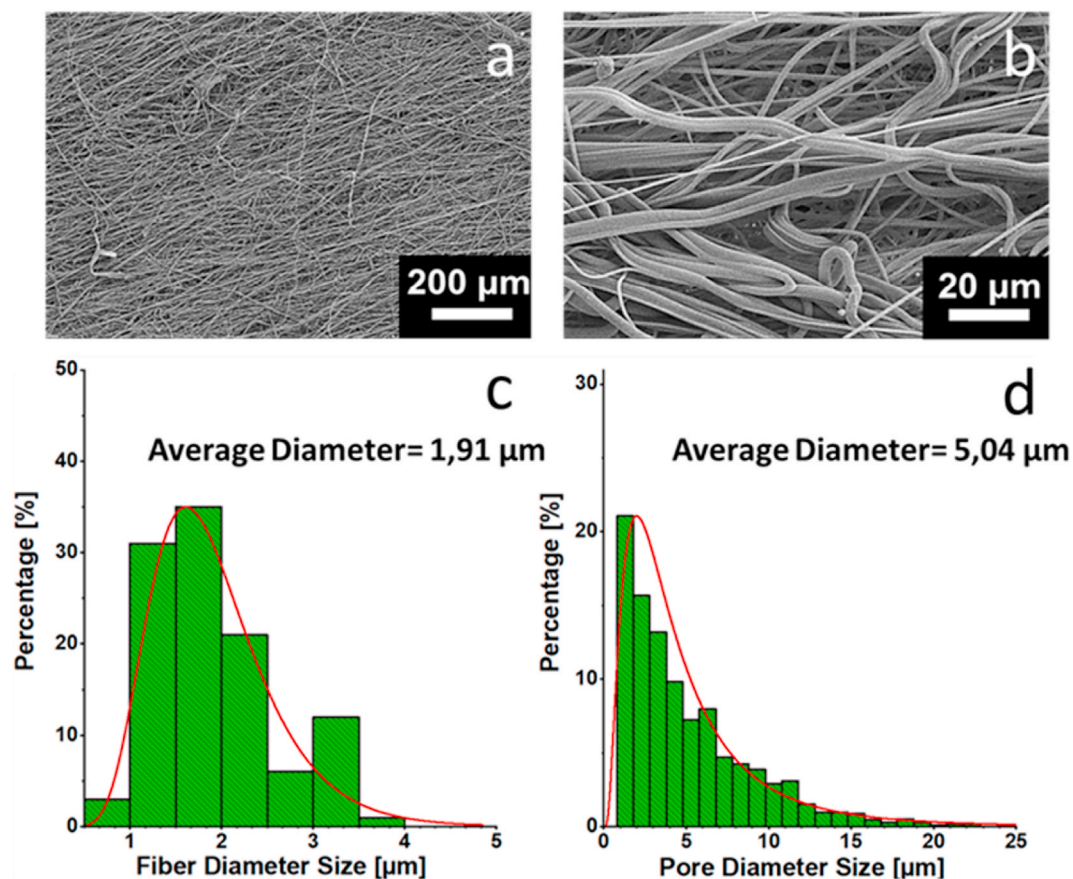
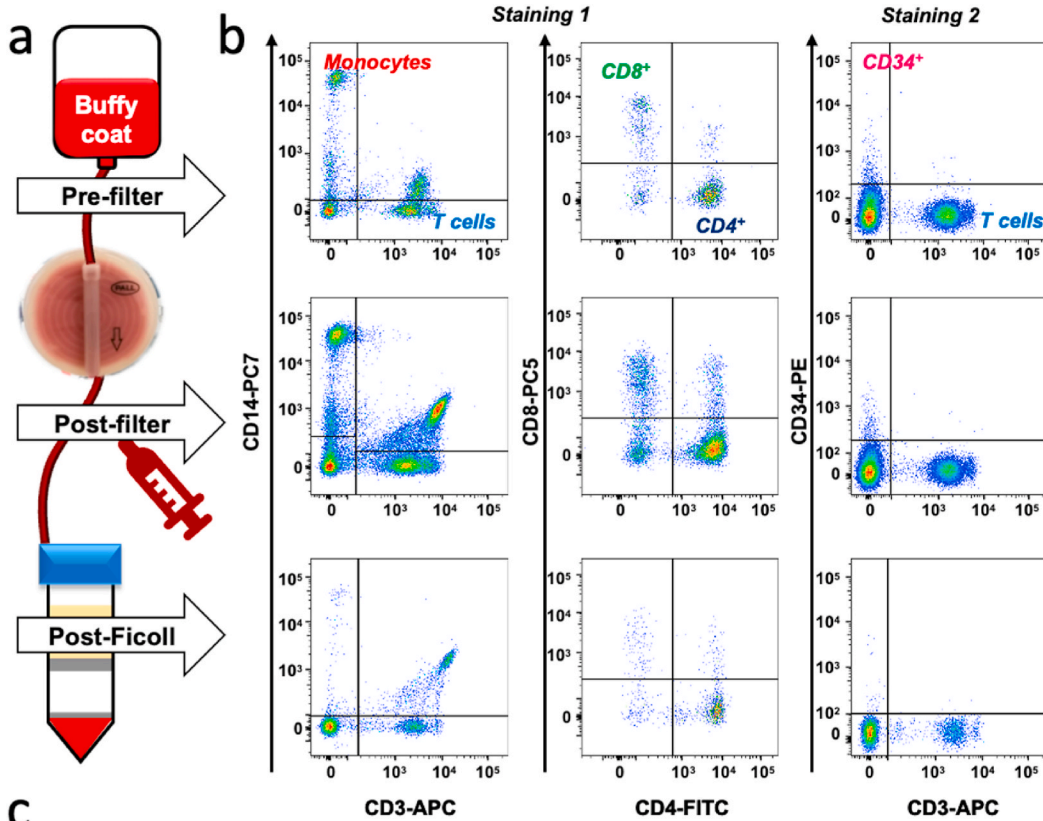
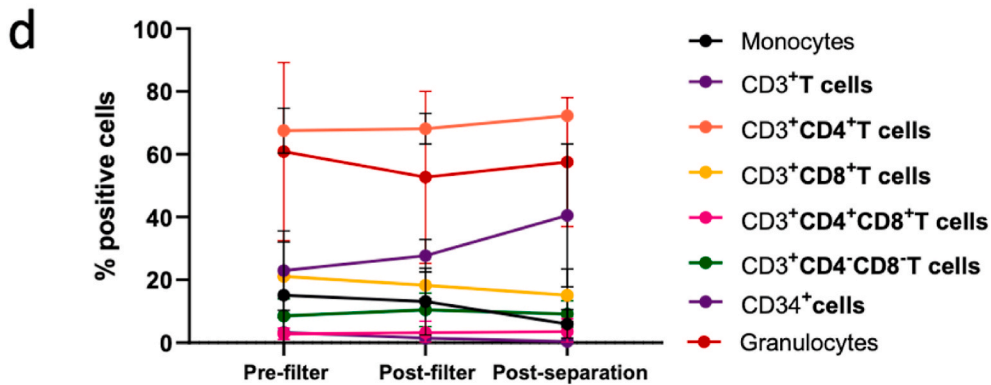


Fig. 2. Filtration system characterization: morphology. SEM images of the filter (A-B); distribution of the fiber diameter size (C); distribution of the pore diameter size (D). Overall, filter structure was homogeneous, with fibers ranging from 0.9 to 4.0 μm (C); this structure is obtainable with melt-blow technology. Pore size distribution (D) was extremely heterogeneous with pores ranging from 1 μm to 20 μm of diameter.



C

	Pre-filter	Post-filter	Post-separation	P value
Monocytes	15.1±16.9%	13.1±10.6%	6±4.5%	0.6490
CD3 ⁺ T cells	22.9±12.7%	27.7±5.2%	40.6±22.7%	0.3762
CD3 ⁺ CD4 ⁺ T cells	67.6±7.1%	68.2±4.9%	72.3±0.1%	0.5062
CD3 ⁺ CD8 ⁺ T cells	21.1±0.1%	18.3±4.2%	15.1±8.3%	0.4891
CD3 ⁺ CD4 ⁺ CD8 ⁺ T cells	2.8±1.8%	3.2±3.7%	3.5±4%	0.5107
CD3 ⁺ CD4 ⁻ CD8 ⁻ T cells	8.5±5.5%	10.4±5.3%	9.1±4.2%	0.7477
CD34 ⁺ cells	3.3±4.6%	1.5±1.7%	0.4±0.3%	0.2875
Granulocytes	66.3±27.4%	52.7±27.3%	57.5±20.6%	0.4901



(caption on next page)

Fig. 3. Flow cytometry immunophenotyping of peripheral blood mononuclear cells. Whole blood was collected and first subjected to filtration and subsequently to Ficoll-Paque density gradient separation (A). Flow cytometry immunophenotyping was performed at each step of the procedure, and frequencies of CD14⁺ monocytes, CD3⁺ T lymphocytes and relative CD8⁺ and CD4⁺ subsets and circulating CD34⁺ hematopoietic stem cells were investigated (B). Percentage of each cell subset was compared before and after filtration and after separation to confirm filter efficacy without losing cells of a particular subset during the procedure (C-D). Data are shown as mean ± SD. A $p < 0.05$ was considered statistically significant.

of PBMCs on modulation of cytokine levels during hBM-MSC myogenic commitment events was also investigated by monitoring cytokine gene expression and protein concentration in culture medium.

2. Results

2.1. Filter characterization

First, commercial filtration system routinely used in clinical practice for autologous transplantation procedures was physically and chemically studied to understand morphological characteristics and composition that make this system suitable for an efficient cell filtration starting from whole blood. Polybutylene terephthalate (PBT) fibers were identified in filter membranes by FTIR spectroscopy (Fig. 1a), showing the presence of terephthalate group, aromatic group, and the stretching of C=O of carbonyl group [37,38]. Profiles of TGA curves evidenced membrane stability up to 350°C both in reactive and inert environment (Fig. 1b), with the main degradation step occurring at around 400°C, due to the breakdown of the polymer in fragments and the formation of combustible gases [37,39]. A very small second step of degradation occurred at around 500°C, more gradually in an inert environment such as nitrogen flow environment, while abrupt in air. Residual profile values at 630°C were similar and almost irrisory. DSC curve showed glass transition of materials at around 30°C and melting temperature at about 223°C (Fig. 1c) [37,39,40].

Moreover, crystallinity degree was evaluated by integration of melting transition as indicated in eq. (1):

$$X_c = \frac{\Delta H_m}{\Delta H_{m,100\%}} = 30.2\% \quad (\text{eq } 1)$$

where ΔH_m is the integrating the melting transition in the DSC curve and $\Delta H_{m,100\%}$ is the melting enthalpy for 100% crystalline PBT, that according to literature is 145.5 J/g [41].

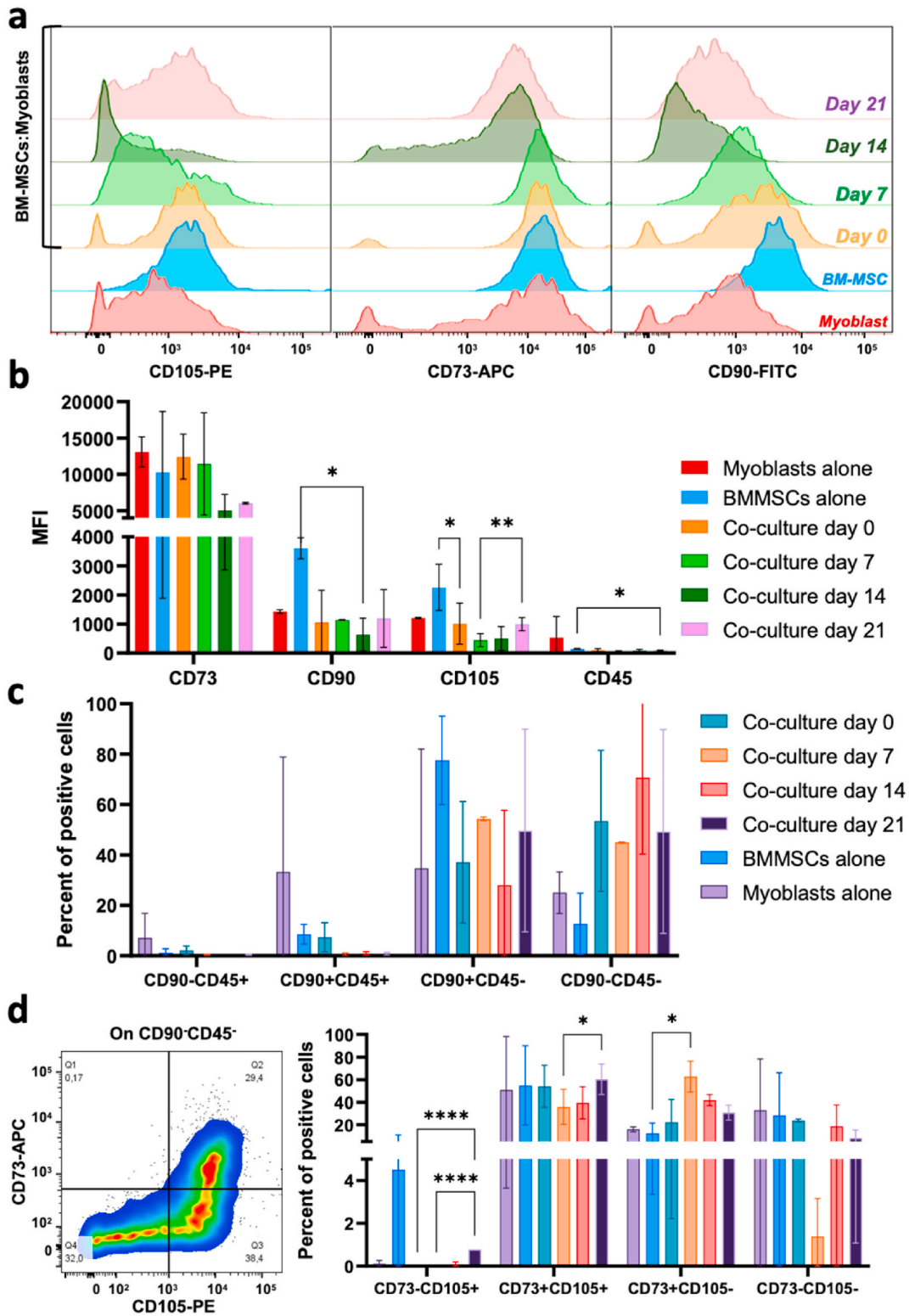
Filter morphology was investigated by Field Emission Scanning Electron Microscope (FE-SEM) (Fig. 2). Overall, filter structure was homogeneous, with fibers ranging from 0.9 to 4.0 μm obtainable with melt-blow technology (Fig. 2c). Pore size distribution (Fig. 2d) was extremely heterogeneous with pores ranging from 1 μm to >20 μm of diameter. Fiber length was of several thousands of millimeters, and clearly visible by optical microscopy (Supplementary Fig. S1). Moreover, the filter had a great water absorption ability and an extremely high hydrophilicity.

2.2. Filtrate composition

To investigate efficacy of the filter to retrieve blood cell populations after filtration, PBMC immunophenotyping was carried out on whole blood, after filtration, and after separation by Ficoll-Paque density gradient, and results were compared (Fig. 3a–b). As expected, no significant variations were described in percentage of positive cells for all studied cell populations, before and after filtration or separation, confirming filter efficiency in blood concentration and composition preservation (Fig. 3c–d). Indeed, starting from a total blood volume of 120 mL, filtrated PBMCs were collected in a final volume of 10 mL of 0.9% saline solution. Therefore, since the relative percentage composition of positive cells was preserved after filtration, cells were concentrated in a final volume 10-times smaller than the starting sample. No differences were observed in percentage of monocytes ($p = 0.6490$), total T cells and T subpopulations (CD3⁺ T cells, $p = 0.3762$; CD4⁺ T cells, $p = 0.5062$; and CD8⁺ T cells, $p = 0.4891$), or granulocytes ($p = 0.4901$), and in percentage of rare circulating cell populations in healthy conditions (e.g., CD34⁺ hematopoietic stem cells, $p = 0.2875$). Those data confirmed filter efficiency in PBMC collection and concentration.

2.3. Effective myogenic commitment of hBM-MSCs: flow cytometry evidence

After confirmed filter efficiency in preserving blood cell population composition, PBMCs were added to a well-established co-culture model of myogenesis to investigate the roles of immune cells on myogenic commitment. First, mesenchymal or myogenic phenotype was confirmed on each single population before further experiments. hBM-MSCs were characterized according to minimal criteria of the International Society of Cellular Therapy [42], while hSkM phenotype was confirmed by gene expression profiling and IF analysis of myogenic markers (e.g., *Pax3*, *MyoD1*, *Myf5*, *Myf6*, *Desmin*, and *MYH2* genes, and Desmin and myosin heavy chain II, or MYH2 proteins, respectively), as previously reported [14]. Subsequently, hBM-MSCs were co-cultured with hSkMs, because the presence of muscle cells highly improves myogenic commitment of mesenchymal cells, as documented [14]. Next, this well-established *in vitro* myogenic commitment model was implemented with filtered PBMCs in transwell, and myogenic events were investigated by flow cytometry immunophenotyping and gene expression profiling at 0, 7, 14, and 21 days, and results were compared or normalized using hBM-MSCs or hSkMs cultured alone (Figs. 4 and 5).



(caption on next page)

Fig. 4. Myogenic commitment of bone marrow-derived mesenchymal stem cells (hBM-MSCs) by flow cytometry analysis. BM-MSCs were co-cultured with myoblasts over 21 days, and myogenic commitment was monitored at day 0, 7, 14, and 21 by investigating variations in mesenchymal and myoblastic marker expression. hBM-MSCs and myoblasts alone were employed as control. Protein expression is reported as normalized cell count histograms (a) or as median fluorescence intensity (MFI) (b) for each studied marker and population over the culture period. MFI of each marker was calculated on single cells in each population and time point, and on hBM-MSCs and myoblasts cultured alone. (c) Variations in frequencies of CD90⁺CD45⁺, CD90⁺CD45⁻, CD90⁺CD45⁻ (hBM-MSC-like phenotype), and CD90⁻CD45⁻ (myocyte-like) cells were investigated throughout the culture, and BM-MSCs and myoblasts cultured alone were used as controls. (d) On myocyte-like population, CD73 and CD105 expression was compared at each time point. Data are shown as mean ± SD. **p* < 0.05; ***p* < 0.01; *****p* < 0.0001.

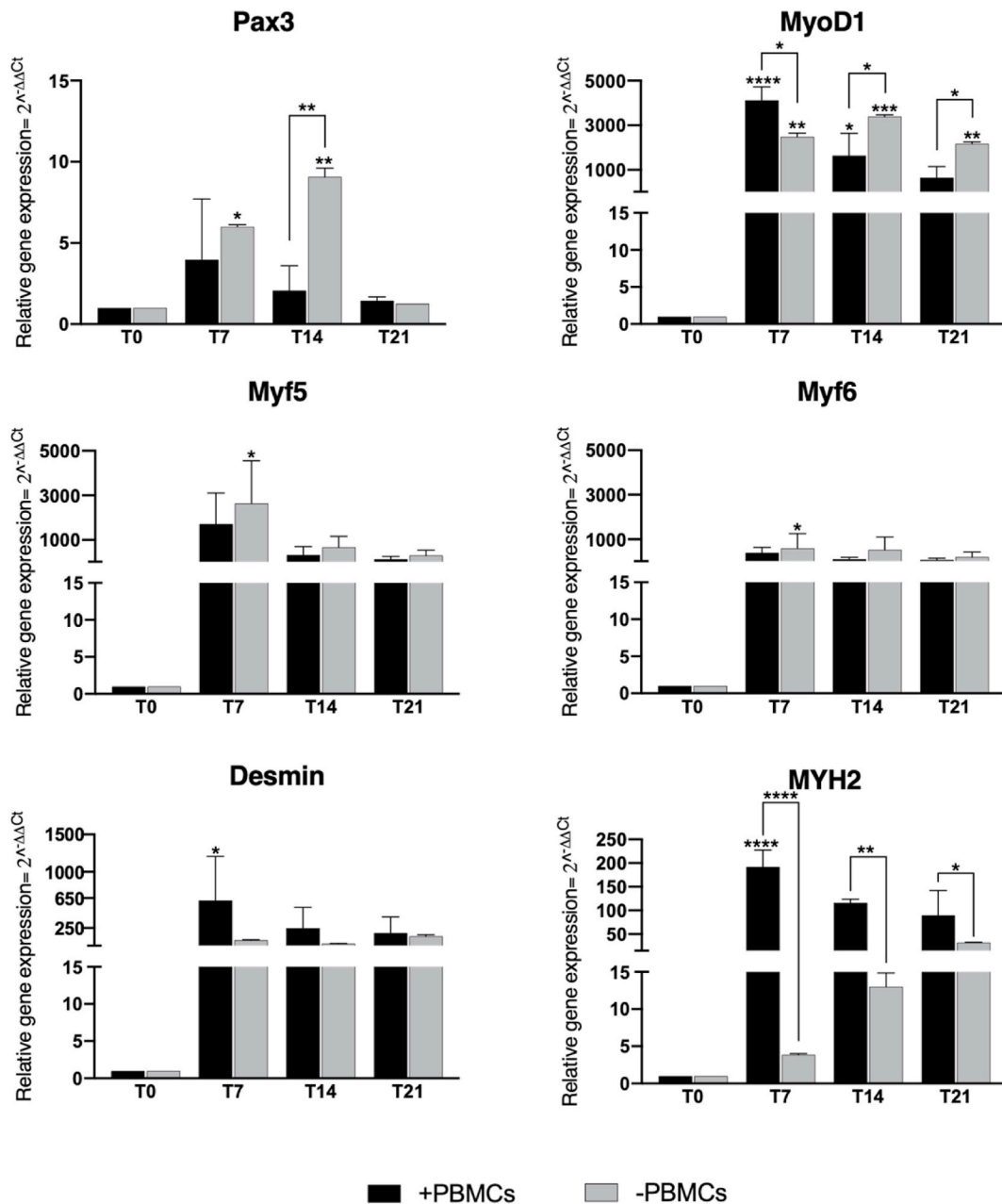


Fig. 5. Gene expression profiling for myogenic markers by quantitative RT-PCR of hBM-MSCs-hSkMs-PBMCs in static culture. hBM-MSCs were co-seeded with hSkMs in ratio 2:1 and PBMCs were culture in the upper chamber of transwell inserts. mRNA levels of myogenic markers: *Pax3*, *MyoD1*, *Myf5*, *Myf6*, *Desmin* and *MYH2* were assayed by qRT-PCR at day 7, 14 and 21 of culture. The relative quantification of each mRNA gene expression normalized to endogenous GAPDH (internal control) was calculated using the $2^{-\Delta\Delta C_t}$ method and presented as fold change over hBM-MSCs at day 0, selected as a control.

In single population cultures, *hBM-MSC* mesenchymal phenotype was confirmed as cells showed positivity for CD90, CD73, and CD105, and negativity for CD45, and *hSkMs* were CD73⁺CD45⁺CD90^{+/-}CD105⁻ (Supplementary Fig. S3). At baseline, co-cultured cells were predominantly CD90⁺CD73⁺CD105⁺CD45⁻, and CD45 negativity and CD73 positivity were maintained throughout the culture (Fig. 4a); while CD90 expression was significantly reduced at day 14 compared to *hBM-MSCs* cultured alone ($p = 0.0310$) (Fig. 4b). CD105 expression was significantly decreased at baseline compared to *hBM-MSCs* cultured alone ($p = 0.0328$) likely because of the co-presence of CD105⁻ myoblasts; however, CD105 levels increased again from day 7 to day 21 ($p = 0.0023$) (Fig. 4b). Therefore, at the end of culture, *hBM-MSCs* switched from a mesenchymal to a mature functional myocyte CD90⁻CD73⁺CD105^{+/-}CD45⁻ phenotype [43].

Next, *hMSC* subset composition variations were monitored throughout the culture by flow cytometry (Fig. 4c-d and Supplementary

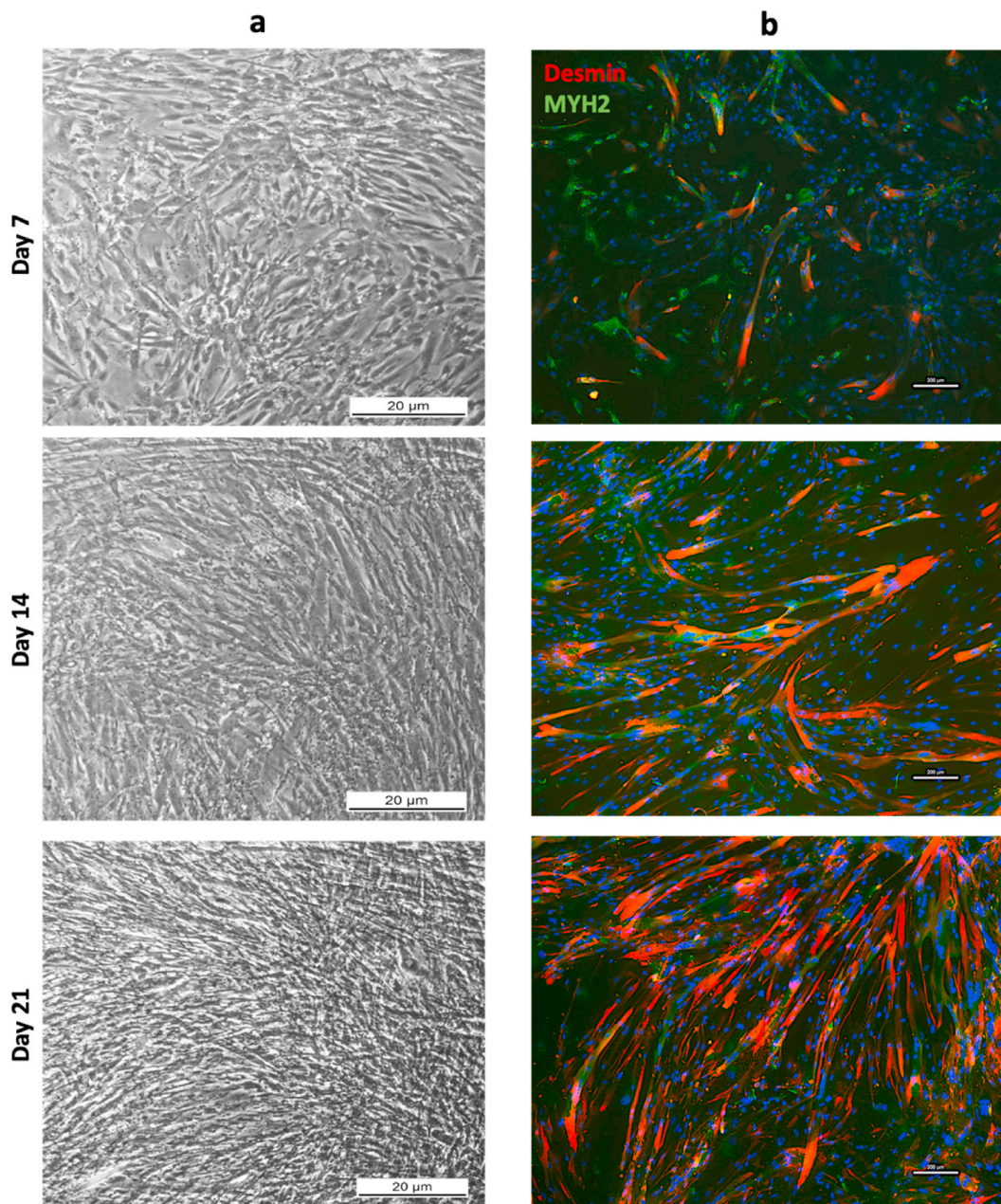
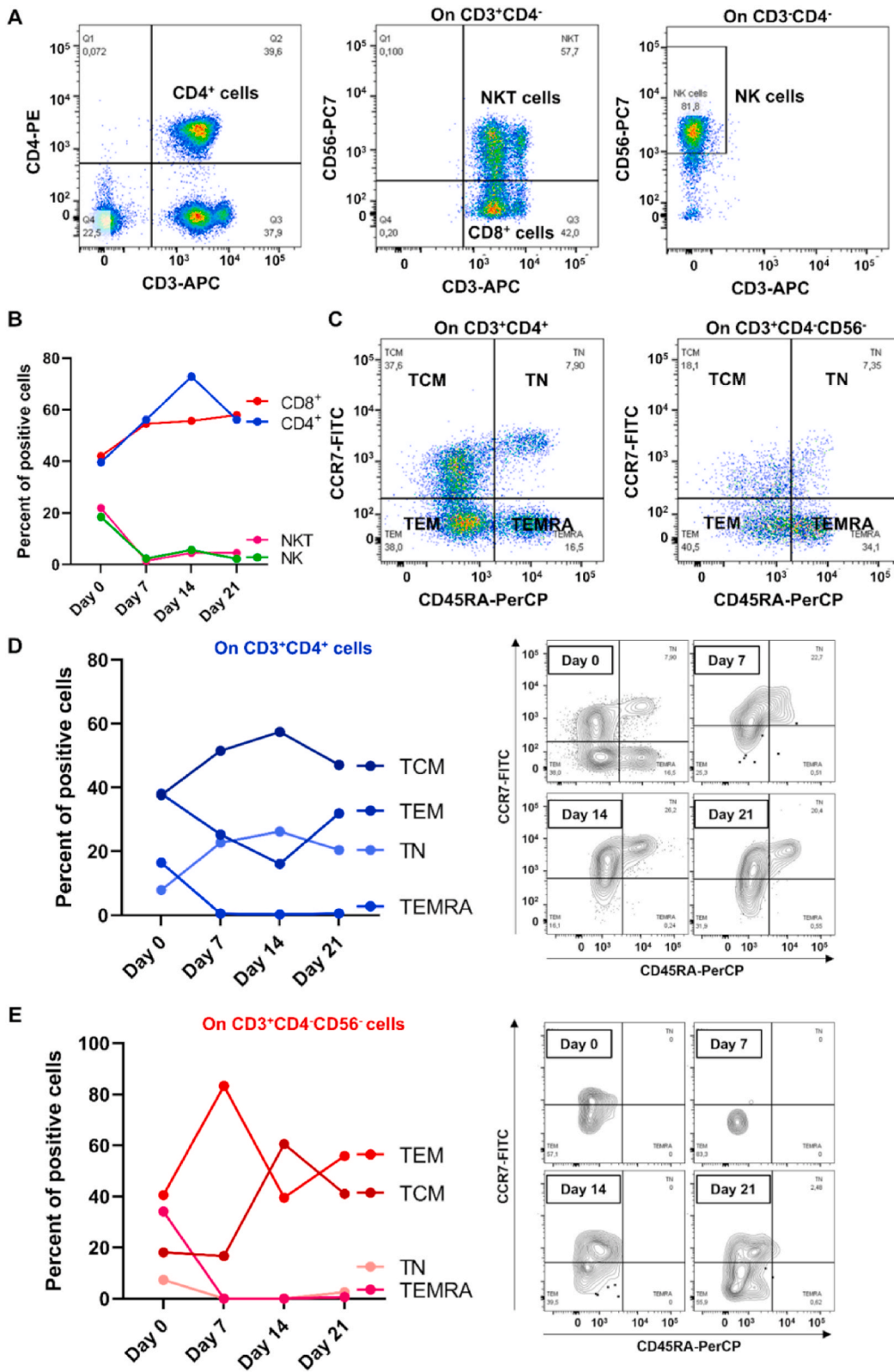


Fig. 6. Brightfield and Immunofluorescence images of *hBM-MSCs*:*hSkMs* 2:1 co-seeded with PBMCs in upper chamber of transwell insert. Brightfield images *hBM-MSCs*:*hSkMs* 2:1 co-seeding culture at day 7, 14 and 21 were captured using 5× magnification; scale bar: 20 μm (a). IF assay was performed at same time points by staining Desmin in red and MYH2 in green (b). All images were captured using 10× magnification, scale bar: 200 μm.



(caption on next page)

Fig. 7. Flow cytometry immunophenotyping of peripheral blood mononuclear cells (PBMCs) in transwell. First, CD4⁺, CD3⁺CD4⁻CD56⁻ (assumed as CD8⁺ T lymphocytes), CD3⁻CD56⁺ Natural Killer (NK), and CD3⁺CD56⁺ NKT cells were identified (a), and perturbations were monitored throughout the culture (b). On CD4⁺ and CD8⁺ T cells, T central memory (TCM), T naïve (TN), effector memory cells re-expressing CD45RA (TEMRA), and effector memory T (TEM) cell subsets were studied (c) and monitored along the culture (d-e).

Fig. S5). No differences in frequencies of CD90⁺CD45⁺, CD90⁺CD45⁻, CD90⁻CD45⁺, or CD90⁻CD45⁻ cells were observed, even though CD90⁻CD45⁻ cell subset tended to increase from day 7 of culture compared to hBM-MSCs ($p = 0.1671$) or hSkMs ($p = 0.1757$) cultured alone (Fig. 4c). On each subset, CD73 and CD105 expression was further investigated, and percentage of positive cells were compared. On CD90⁺CD45⁺ cells (likely myoblasts), no significant variations in CD73⁻CD105⁺, CD73⁺CD105⁺, CD73⁺CD105⁻ (myoblast phenotype), or CD73⁻CD105⁻ cell subsets were observed (Supplementary Fig. S5a), suggesting that our 2D culture system did not alter myoblast phenotype. On CD90⁺CD45⁻ subset, CD73⁺CD105⁺ cells (hBM-MSC phenotype) were significantly decreased already after 7 days of culture compared to baseline ($p = 0.0463$) and to hBM-MSCs cultured alone ($p = 0.0062$); while CD73⁺CD105⁻ cell (committed hBM-MSC) frequency was significantly increased starting from day 7 compared to baseline ($p = 0.0486$) and to hBM-MSCs cultured alone ($p = 0.0236$) (Supplementary Fig. S5b), suggesting that after 7 days of culture, hBM-MSCs lost their stemness and started to differentiate toward the myogenic lineage. Finally, on CD90⁻CD45⁻ subset, terminally differentiated CD73⁺CD105⁺ myocytes were significantly increased at the end of culture compared to day 7 ($p = 0.0351$); however, immature functional CD73⁺CD105⁻ myocytes were already significantly augmented after 7 days of culture compared to hBM-MSCs cultured alone ($p = 0.0417$) (Fig. 4d).

2.4. Effective myogenic commitment of hBM-MSCs: gene expression profiling

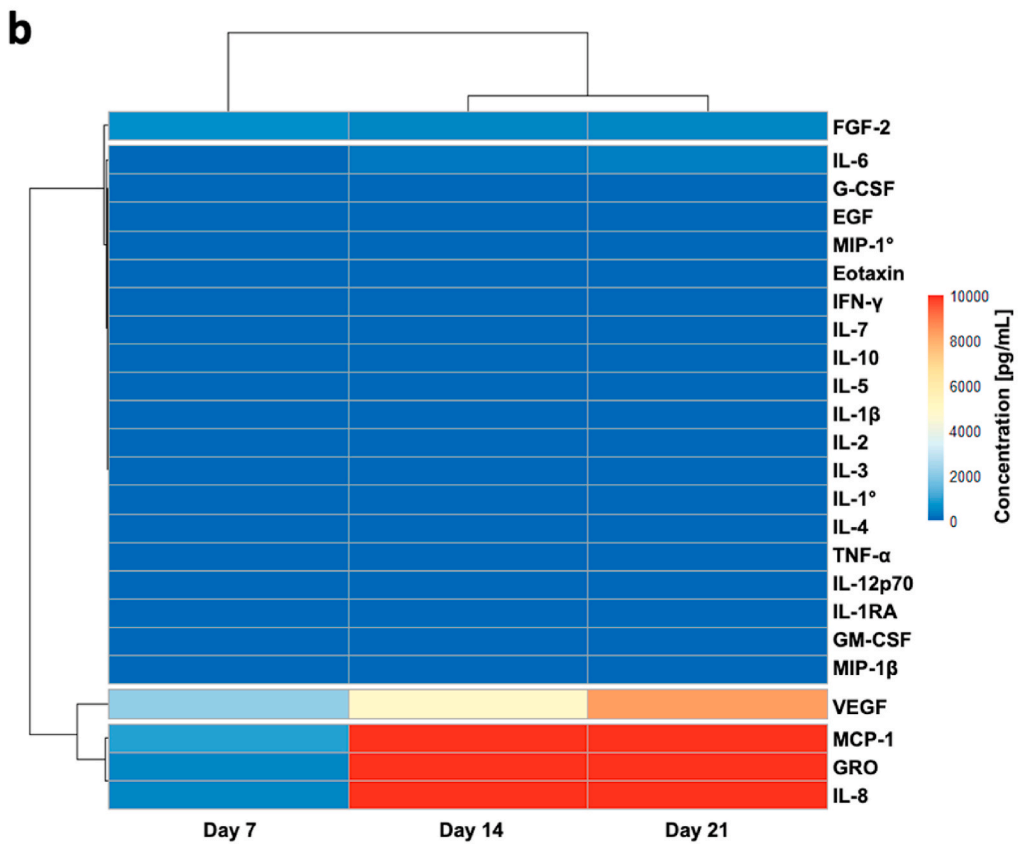
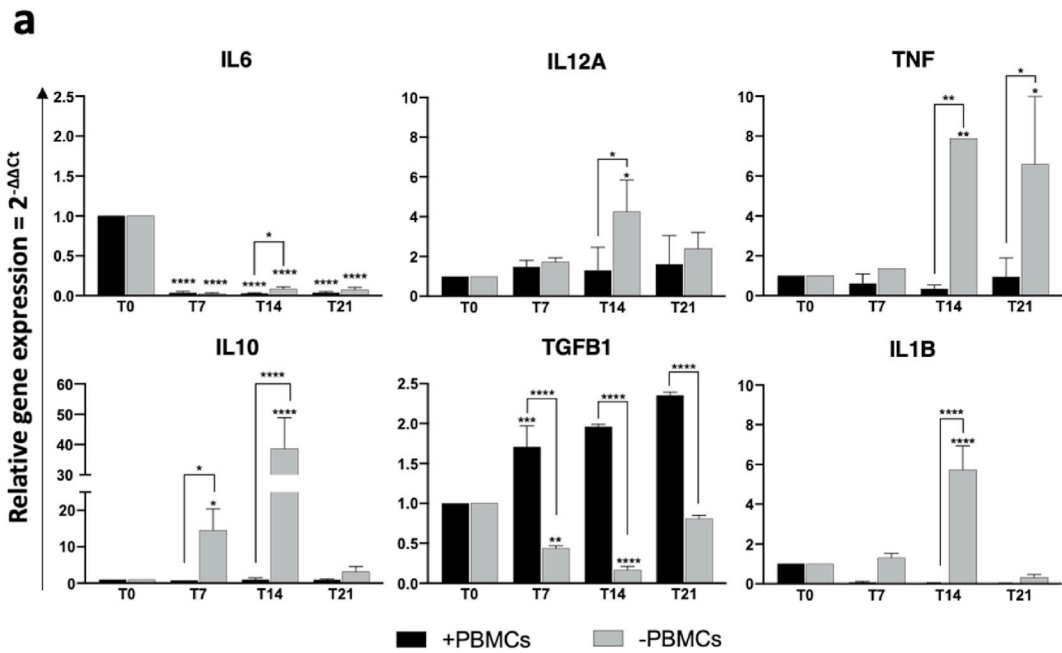
Subsequently, gene expression profiling of myogenic markers including *Pax3* and myogenic-related factors (MRFs; *MyoD1*, *Myf5* and *Myf6*) was studied on hBM-MSC-hSkM co-seeding culture with and without PBMCs (Fig. 5). *Pax3*, *Myf5*, and *MyoD1* were considered as satellite cell/myoblast markers, while *Myf6* and *MYH2* as mature myocyte markers. *Pax3*, the *Pax7* paralogue, is expressed in skeletal muscle cells in both quiescent and activated status [44]. *Pax3* was up-regulated of 4- and 6-folds ($p < 0.05$) in the presence or absence of PBMCs at day 7, respectively. At day 14, the expression resulted significantly higher without PBMCs (9.1-fold, $p < 0.01$) while at day 21, cells showed similar *Pax3* expression levels regardless the presence of PBMCs. *MyoD1* expression levels at day 7 was about 4124-fold, ($p < 0.0001$) then decreased at 1638-fold ($p < 0.05$) with PBMCs; whereas, in culture without PBMCs, *MyoD1* expression reached 2489-fold ($p < 0.01$) at day 7 but increased at 3397-fold ($p < 0.001$) at day 14. At day 21, in both conditions, the expression showed a decreasing trend to 644.5-fold with PBMCs and 2165-fold without PBMCs with significant differences between the two data set ($p < 0.05$). In the presence of PBMCs, *Myf5* was upregulated at 1709-fold, while without them the expression was about 2640-fold ($p < 0.5$), at day 7. Then the expression decreased in both culture conditions, about 320-fold and 126-fold with PBMCs and 671-fold and 302-fold without, at day 14 and 21 respectively. The maximum fold-change of *Myf6* occurred at day 7, about 388-fold with PBMCs and 590-fold without PBMCs ($p < 0.5$). At day 14 and 21, the expression showed almost the same values, 100-fold and 73-fold with respect to 525-fold and 200-fold without PBMCs. *Desmin* was significantly up-regulated in the presence of PBMCs at day 7 with from 619-fold, ($p < 0.5$), to 200-fold at day 21, compared to cells cultured without PBMCs that showed an upregulation of 87.3-fold at day 7 and of 141-fold at day 21. Similarly, *MYH2* gene expression levels were significantly higher in the presence of PBMCs compared to cells cultured without PBMCs (192-fold vs 3.8-fold, $p < 0.0001$, at day 7; 116-fold vs 13-fold, $p < 0.01$ at day 14, and 89.6-fold vs 32.4-fold, $p < 0.5$, at day 21).

hBM-MSC-hSkM cell morphology in the presence of PBMCs was monitored in brightfield optical microscope at each time point and elongated and proliferating cells were displayed starting from day 7 (Fig. 6a). More growing cells, longitudinally organized in parallel bundles, were documented along the culture period together with increasing protein expression of Desmin and MYH2, as observed by IF assay (Fig. 6b).

2.5. Pro-inflammatory activities of T effector memory lymphocytes and Natural Killer cells could negatively influence myogenic commitment

Based on our results showing a better myogenic commitment of hBM-MSCs in the presence of PBMCs and on the role of immune system in modulating muscle injury repair [30], we explored the influence of PBMCs on myogenic commitment of co-cultured hBM-MSCs and hSkMs by flow cytometry immunophenotype of isolated PBMCs (post-separation) in transwell and gene expression profiling of pro- and anti-inflammatory cytokines (Figs. 7 and 8). CD4⁺, CD3⁺CD4⁻CD56⁻ (assumed as CD8⁺ cells), Natural Killer (NK), and NKT cell frequencies were monitored throughout the culture (Fig. 7a), and NK and NKT cells tended to decrease already after 7 days of culture, while CD8⁺ and CD4⁺ T cells tended to increase and to reach a plateau from day 14–21 of culture (Fig. 7b). T cell central memory (TCM), T naïve (TN), T effector memory re-expressing CD45RA (TEMRA), and T effector memory (TEM) subset frequencies were monitored along the culture in CD4⁺ and CD8⁺ T lymphocytes (Fig. 7c). On CD4⁺ T cells, TEMRA and TEM cells tended to decrease after 7 or 14 days of culture, while TCM and TN cells increased, being TCM the predominant CD4⁺ T cell subset (Fig. 7d). On CD8⁺ T cells, TN and TEMRA were almost absent at the end of culture, while TCM markedly increased from day 7 and TEM decreased, being these two subsets the most predominant in CD8⁺ T cells at the end of culture (Fig. 7e).

Next, cytokine expression in co-culture system was investigated by qRT-PCR in the presence or not of PBMCs (Fig. 8a). All pro-inflammatory cytokines showed very low expression levels in the presence of PBMCs, such as *IL12A* reached 1.3-fold vs 4.3-fold at



(caption on next page)

Fig. 8. Pro- and anti-inflammatory cytokine expression by quantitative RT-PCR and immunoassay in static hBM-MSC-hSkM-PBMC co-culture. (a) hBM-MSCs were co-seeded with hSkMs in ratio 2:1 and PBMCs were culture in the upper chamber of transwell inserts. mRNA levels of pro-inflammatory (*TNF*, *IL12A*, and *IL1B*) and anti-inflammatory cytokines (*IL10*, *TGFB1*, and *IL4*) were assayed by qRT-PCR at day 7, 14 and 21 of culture. The relative quantification of each mRNA gene expression normalized to endogenous GAPDH (internal control) was calculated using the $2^{-\Delta\Delta Ct}$ method and presented as fold change over hBM-MSCs at day 0, used as control. (b) Cytokine levels were also measured in culture medium supernatants at day 7, 14, and 21 by magnetic bead-based multiplex immunoassay. Data are reported as heatmap from blue (lowest value, 0 pg/mL of concentration) to red (highest value). Cytokines were hierarchical clustered based on expression pattern. Heatmap was made using *Pheatmap* and *ComplexHeatmap* packages in R Studio software (v. 2022.07.1 + 554; R Studio, Boston, MA, US). * $p < 0.05$; ** $p < 0.01$; *** $p < 0.0001$.

day 7, $p < 0.5$, with and without PBMCs respectively. *TNF* was also significantly upregulated at day 14 in the absence of PBMCs (4.5-fold, $p < 0.1$, vs 0.35-fold without and with PBMCs, respectively); as well as at day 21, the presence of PBMCs resulted in a significantly *TNF* downregulation (6.6-fold vs 0.9-fold, with and without PBMCs, respectively; $p < 0.1$). Similarly, anti-inflammatory cytokines, such as *IL10*, were significantly upregulated in hBM-MSCs-hSkMs cultured in the absence of PBMCs (38.6-fold, $p < 0.0001$), completely lost in the presence of PBMCs. Interestingly, *TGFB1* showed a different expression profiling, compared to other investigated cytokines, as hBM-MSCs-hSkMs cultured in the presence of PBMCs displayed a significant upregulation of *TGFB1* throughout the culture period (from 1.6-fold at day 7 to 2.3-fold at day 21), while poorly expressed in the absence of PBMCs. *IL4*, *IL6*, *IFNG* and *TGFB2* were not detected in any conditions.

Cytokine secretion was also investigated by analyzing culture medium supernatants at 7, 14 and 21 days by magnetic bead-based immunoassay (Fig. 8b). Among 24 cytokines studied, only monocyte chemoattractant protein-1 (MCP-1), growth-regulated alpha protein (GRO), and IL-8 were significantly high in culture medium starting from day 14, while vascular-endothelial growth factor (VEGF) reached the pick at the end of culture. All the other studied cytokines were not present in culture medium supernatants.

3. Discussion

Regenerative procedures are routinely used in clinical practice for supporting tissue healing. In CLI or other critical ischemic lesions, self-revascularization ability of resident stem cells is limited, and autologous transplantation of PBMCs concentrated by blood filtration with commercial filter systems (e.g., HeMaTrate®) can improve myofiber and vascular regeneration leading to limb rescue in CLI patients [1–3]. However, the exact mechanism by which autologous PBMCs support both muscle and vascular healing in CLI is still unclear. Indeed, the exact role of PBMCs in influencing myogenic events is still under debate, even though pharmacological targeting of inflammation and immune functions result in faster healing processes. In case of severe injuries, skeletal muscle capacity to spontaneously heal appears insufficient, and available treatments do not provide optimal restoration to preinjury status [8]. Therefore, biological treatments, including cell therapy and tissue engineering protocols, are of clinical interest, and a biomimetic *in vitro* model could be a precious tool to better understand the complex mechanism behind healing processes to improve clinical management. In this work, we implemented our previously established myogenic model based on hBM-MSC-hSkM co-culture by adding PBMCs collected by a commercial filtration system to explore their potential contribution to myogenic commitment of hBM-MSCs. In our experience, myogenic commitment is highly enhanced by the presence of myoblasts, likely because of cell-to-cell contacts and secreted factors favoring myogenic differentiation of MSCs [14]. So that, PBMCs were implemented in this well-established *in vitro* myogenic model adopting a transwell chamber to investigate the role of paracrine factors released by inflammatory cells in tissue repair.

First morphological, physical and chemical properties of the filter were studied to highlight those characteristics that allow an efficient whole blood filtration. Based on filter characterization, cell suspension is retained within the continuous capillary network of the porous structure of the filter medium, likely because of combined actions of several factors, including sedimentation along the tortuous capillary path, chemical-physical filter properties-related adsorption, and electrostatic attraction between the opposite electric charges of cells and filter medium materials.

Filtered fractions were composed by all peripheral blood mononucleated populations, such as granulocytes, monocytes, lymphocytes, and stem cells – a rare circulating population in healthy individuals –, without significative differences in relative percentage before and after filtration, even in T cell subpopulation distribution, as already described, confirming filter efficiency in filtration and blood composition preservation [45], as well as blood concentration from a starting total whole blood volume of $98.2 \text{ mL} \pm 8.49$ to a final enriched concentrate volume of $12.84 \pm 1.29 \text{ mL}$ (7 times enriched) [45]. Similarly, we efficiently concentrate whole blood starting from a total volume of 120 mL to a filtrated PBMC volume of 10 mL in 0.9% saline solution, with a higher yield of enrichment (10 times) compared to previously reported data.

Isolated PBMCs were added to hBM-MSC-hSkM co-cultures developing a novel *in vitro* three-cell co-culture myogenic model. More in details, PBMCs were added in the upper chamber of a transwell insert to study their potential paracrine effects in hBM-MSC myogenic commitment; however, their presence did not significantly influence the expression of myogenic transcription factors, while *Desmin* and *MYH2* were significantly upregulated already after seven days of cultures compared to co-culture without PBMCs. Our data suggest that PBMCs might release factors that can significantly speed-up hBM-MSC commitment toward the myogenic phenotype, as markers of a more mature myocytic phenotype (e.g., *MyoD1*, *Desmin*, and *MYH2*) were significantly upregulated just after seven days of culture compared to co-culture without PBMCs that upregulated later in culture myocytic markers (e.g., *MYH2* at 21 days of culture).

Successful myogenic commitment was also confirmed by flow cytometry immunophenotyping and IF analysis, as CD90 negativization mirrored lineage commitment of hBM-MSCs toward $\text{CD90}^- \text{CD73}^+ \text{CD105}^{+/-}$ mature myocytes as well as the expression of *Desmin* and *MYH2* at protein level.

During myogenesis and skeletal muscle regeneration, a broad range of cytokines are secreted by stem cells, muscle cells and

immune cells. First pro-inflammatory cytokines and then anti-inflammatory ones increase transiently triggering myogenesis cascade events. Cytokines coordinate inflammatory response, induce additional immune cell recruitment, and allow the complex cell-cell crosstalk, favouring muscle healing and maintaining healthy physiological condition [14,30].

We previously demonstrated that pro-inflammatory cytokines were upregulated, regardless the presence of low concentrations of glucocorticoids in the supplemented medium [46]. Here, we observed that only *TGFBI* was significantly upregulated by co-cultured cells in the presence of PBMCs, while *IL12A*, *TNF*, *IL10*, and *IL1B* expression was significant increase in *hBM-MSK-hSkM* co-culture in the absence of peripheral blood cells. *TGFBI* is considered an inhibitor of muscle differentiation through MyoD1 inactivation [47]; however, our results showed a high upregulation of *MyoD1* along the culture, thus the modest upregulation of *TGFBI* could be due to its contribution to a transient matrix deposit [48,49]. Conversely, macrophage chemoattractants and growth factors, such as GRO, MCP-1, IL-8, and VEGF, were increasingly present in medium along the culture. Indeed, during myogenesis and muscle healing, chemoattractant factors play a pivotal role in cell recruitment like phagocytes, without which the process progression is destined to stop [30]. VEGF, a well-known neovascularization growth factor and also a therapeutic target in cancer treatments, is involved in muscle tissue regeneration by favoring blood vessel neofunction, and by muscle cell proliferation [50,51]. Moreover, PBMCs might not be the principal source of TNF in our myogenic model; indeed, when adopting same *in vitro* co-culture system, in absence of PBMCs TNF is significantly upregulated throughout the culture, as described elsewhere [52].

As a consequence, PBMCs might exert an anti-inflammatory paracrine effect on microenvironment composition that could favor *hBM-MSK* myogenic commitment and might also create an optimal chemoattractant gradient that might favor macrophage and neutrophil recruitment for clearance of debris and for induction of healing processes after traumatic injuries.

In conclusion, this novel three-cell co-culture *in vitro* system allowed the investigation of paracrine effects of PBMCs on myogenic commitment of *hBM-MSKs*. Our results show that the presence of immune cells could improve differentiation of *hBM-MSKs* toward the myogenic phenotype and could promote an anti-inflammatory and phagocyte-permissive microenvironment thus improving both cell proliferation and clearance of debris, especially in muscle injuries. Our *in-vitro* model also opens perspectives for a more comprehensive exploration of MSC behavior along myogenic commitment and for better studying the complex crosstalk between stem and immune cells, likely favoring regeneration events. However, our data need further *in vivo* and *in vitro* investigations to better understand the exact role of PBMC or specific immune cell subsets on myogenesis and healing events, and to identify a possible pharmacological target. Moreover, proposed data open new scenarios for future use of these blood filtration system to collect PBMC fraction to treat severe muscle injuries and to accelerate healing events in clinical practice, as these filter devices could represent a valid and alternative therapeutic option in muscle regenerative medicine.

4. Limitations of the study

In this study, we performed a structural and functional analysis of a filtration system routinely used in clinical practice for autologous cell transplantation from blood, exploring *in vitro* the roles of PBMC fraction in myogenesis events. Even if a well-established *in-vitro* model of co-culture of human skeletal muscle cells and stem cells from bone marrow was adopted, further *in vivo* evaluation may be necessary to better understand the role of PBMC fraction in muscle healing events.

5. Methods

5.1. Filter characterization

Filter system HeMaTrate (CH-WB110C, Patent n. EP 2602315A1) was supplied by Pall Medistad B.V. (Medemblik; Netherlands) for Cook Regentec (Indianapolis, Indiana, USA), and fiber characteristics were determined by optical microscope and Field Emission Scanning Electron Microscope (FE-SEM). Pore size distribution was obtained by converting FE-SEM images to binary using MATLAB software, as previously published [53,54].

More details are described in Supplementary Material and shown in [Supplementary Fig. S1](#). Spectroscopical, thermal and morphological characteristics were also investigated ([Supplementary Material](#)).

5.2. PBMC concentration with filtration system and harvesting

Whole peripheral blood obtained from three healthy volunteers (a female and two males; age ranged from 38 to 45 years old) was concentrated using a blood filtration system (HeMaTrate®, Pall Medical Corporation) as per manufacturers' instructions ([Supplementary Fig. S2](#)). PBMCs were further isolated using Ficoll-Paque density gradient centrifugation (Cytiva, Marlborough, MA-USA), according to manufacturer's instructions. Isolated cells were directly used for flow cytometry immunophenotyping or stored in 70% RPMI (Gibco™), 20% Fetal Bovine Serum (FBS, Gibco™), and 10% DMSO (Sigma-Aldrich, Milan, Italy) at -80°C until use.

5.3. hBM-MSK isolation, harvesting and characterization

BM specimens for isolation of *hBM-MSKs* were obtained from three healthy male donors (aged 26, 24 and 28 years old) after informed written consent in accordance with protocols approved by our Institutional Review Board (Ethic Committee "Campania Sud", Brusciano, Naples, Italy; prot./SCCE n. 24,988). Isolation and characterization were performed as previously documented and according to the International Society of Cellular Therapy guidelines ([Supplementary Material](#) and [Supplementary Fig. S3a](#)) [42].

5.4. Flow cytometry

MSC and PBMC immunophenotype was investigated by flow cytometry on both fresh and frozen samples. Briefly, for hBM-MSCs, a minimum of 1×10^5 cells at the third passage was stained with antibodies listed in [Supplementary Table S1](#) and as previously described [52,55]. Cells were incubated at room temperature (RT) for 20 min in the dark, washed with phosphate buffered saline (PBS, Gibco™) and resuspended in 300 μ L of the same buffer for acquisition. For PBMC immunophenotyping, before and after filtering and separation procedures, a minimum of 2×10^5 cells were stained with antibodies listed in [Supplementary Table S1](#). For immunophenotyping of PBMCs in transwell at day 0 ([Supplementary Fig. S4](#)) a minimum of 2×10^5 cells were stained antibodies listed in [Supplementary Table S1](#). Cells were then incubated at RT for 20 min in the dark, washed with PBS and resuspended in 300 μ L of the same buffer for acquisition. Sample acquisition was performed on a BD FACSVerser flow cytometer (Becton Dickinson, BD, NJ, USA) equipped with blue (488 nm) and red lasers (628 nm) and BD FACSuite software (BD Biosciences). PMT voltage setting, and compensation were carried out using single-color controls for each fluorochrome and an unstained sample as negative control. All samples were run with the same PMT voltages, and a minimum of 30,000 events were recorded. FlowJo software (v.10.7.1, LLC, BD Biosciences) was employed for post-acquisition compensation and analysis.

hBM-MSCs were first identified using linear parameters (forward scatter area (FSC-A) vs side scatter area (SSC-A), and double cells were excluded (area vs height, FSC-A vs FSC-H) ([Supplementary Fig. S5](#)). On single cells, CD90 and CD45 expression was explored, and CD90⁺CD45⁻ cells were further studied for CD105 and CD73 expression. Similarly, on single cells, HLA-DR and CD34 expression was investigated, and CD34⁻HLA-DR⁻ cells were further studied for CD14 expression. During co-culture, CD105 and CD73 expression was monitored in CD90⁺CD45⁺, CD90⁺CD45⁻, and in CD90⁻CD45⁻ cells.

For PBMC immunophenotyping before and after filtration and after separation, debris were excluded using linear parameters (FSC-A vs SSC-A), and double cells removed (FSC-A vs FSC-H). On single cells, CD3 and CD14 expression was first investigated, and CD14⁺ monocytes and CD3⁺T cells were identified. On T cells, CD4 and CD8 expression was further studied, and CD4⁺, CD8⁺, double positive CD4⁺CD8⁺, and double negative CD4⁻CD8⁻ T cells were identified. For immunophenotyping of PBMCs in transwell during co-cultures, on single cells, CD3 and CD4 expression was investigated, and CD3⁺CD4⁺ cells were gated and further studied for CD45RA and CCR7 expression. On CD3⁺CD4⁻ cells, CD56 expression was investigated (CD56 vs CD3), and Natural Killer (NK) T cells were identified (CD3⁺CD56⁺ cells), while CD3⁺CD4⁻CD56⁻ cells were assumed as CD8⁺ T cells and CD45RA and CCR7 expression was studied. On CD3⁻CD4⁻ cells, NK cells were identified as CD3⁻CD56⁻ cells. T central memory (TCM) cells were defined as CCR7⁺CD45RA⁻, T naive as CCR7⁺CD45RA⁺, effector memory cells re-expressing CD45RA (TEMRA) T cells as CCR7⁻CD45RA⁺, and effector memory T cells (TEM) as CCR7⁻CD45RA⁻, as previously described [52,55].

5.5. hBM-MSC-hSkM-PBMC static co-culture

hBM-MSCs and hSkMs were co-seeded at a density of 4000 cells/cm² and at 2:1 ratio in a 12-well plate containing a differentiation medium composed by: 67% of α -MEM supplemented with 1% Glutagro™, 10% FBS (Gibco™), 100 nM Dexamethasone (Sigma-Aldrich), 100 μ M Ascorbic Acid (Sigma-Aldrich), 10 ng/mL basic fibroblast growth factor (Peprotech, Rocky Hill, New Jersey, United States), and 1% Penicillin/Streptomycin (Corning, Manassas, VA, United States), and 33% of DMEM low glucose (Gibco™) supplemented with 2% Horse Serum (Gibco™), 100 nM Dexamethasone (Sigma-Aldrich), 100 μ M Ascorbic Acid (Sigma-Aldrich), 10 ng/mL bFGF (Peprotech), and 1% Penicillin/Streptomycin. Fresh PBMCs were seeded at day 0 at a density of 10,000 cells/well in the upper chamber of transwell inserts, composed by a semi-permeable membrane with a pore size of 0.4 μ m. At each time point, frozen PBMCs were thawed and added to co-culture system. Cells were incubated at 37 °C in an atmosphere of 5% CO₂ and 95% relative humidity up to 21 days, fresh medium was changed every three days. Brightfield images of hBM-MSC-hSkM co-cultures were captured at 5 \times magnification at 7, 14 and 21 days by LEICA DMIL LED microscope (Leica Microsystems GmbH, Wetzlar, Germany), and acquired using a LEICA DFC425C camera.

5.6. RNA isolation and gene expression profiling

Myogenic (*Pax3*, *MyoD1*, *Myf5*, *Myf6*, *Desmin*, and *MYH2*) and cytokine (*IL6*, *TNF*, *IL12A*, *IL1B*, *IFNG*, *IL10*, *IL4*, *TGFB1* and *TGFB2*) (all from Bio-Rad, Foster City, CA, USA; [Supplementary Table S2](#)) gene expression was investigated by Reverse Transcription quantitative polymerase chain reaction (RT-qPCR) ([Supplementary Material](#)). Experiments were run in duplicate. Data were normalized to glyceraldehyde-3-phosphate dehydrogenase (*GAPDH*) expression (reference gene) applying the geNorm method [56] and using CFX Manager software ($M < 0.5$). Fold changes were determined by 2^{- $\Delta\Delta$ Ct} method and presented as relative levels versus untreated cells.

5.7. Cytokine detection

For quantification of secreted cytokines in culture medium, a multiplex immunobead-based multiplex assay (Merck, Millipore) was employed for measurement of EGF, Eotaxin, GM-CSF, IFN- γ , IL-10, IL-12p70, IL-1RA, IL1a, IL-1b, IL-2, IL-3, IL-4, IL-5, IL-7, MIP-1a, MIP-1b, TNF- α , bFGF, G-CSF, GRO, IL-6, IL-8, MCP-1, and VEGF, following manufacturer's instructions.

5.8. 2D immunofluorescence assay

Fixed and permeabilized cells were stained for Desmin (1:100; Abcam, Cambridge, UK) and MYH2 (1:50; Thermo Fisher Sci.,

Waltham, MA, USA), and cell nuclei were counterstained using 4',6-diamidino-2-phenylindole (DAPI) (Supplementary Material).

5.9. Statistical analysis

Data were analyzed using Prism software (v.9.0, GraphPad software, LLC, San Diego, California, United States). Results are presented as mean \pm standard deviation (SD). Statistical analysis was performed using two-tailed independent Student's t-test for two group comparisons, or two-way analysis of variance (ANOVA) test for three or more group comparison with Tukey's test for multiple comparisons between group. For flow cytometry data, results are presented as percentage of positive cells, and expression of each marker on single cells is also reported as histograms and using unstained samples as negative controls. Percentage of positive cells and median fluorescence intensity (MFI) values were calculated for each marker. p value < 0.05 was considered statistically significant [57].

Author contribution statement

Pasqualina Scala: Performed the experiments; Analyzed and interpreted the data; Wrote the paper.

Paola Manzo, Raffaele Longo, Bianca Serio: Performed the experiments.

Valentina Giudice: Analyzed and interpreted the data; Wrote the paper.

Maria Camilla Ciardulli: Analyzed and interpreted the data.

Carmine Selleri, Liberata Guadagno, Laura Rehak, Nicola Maffulli: Contributed reagents, materials, analysis tools or data.

Giovanna Della Porta: Conceived and designed the experiments; Analyzed and interpreted the data; Wrote the paper.

Funding statement

Nicola Maffulli and Professor Giovanna Della Porta were supported by University of Salerno {FARB 2021}

This work was supported by Athena Srl 139, Viale Europa - 50,126 Firenze (IT) {"The design and implementation of an 3D bio-engineered model for study on skeletal muscle regeneration and inflammation processes. Year 2020–21}

Data availability statement

Data will be made available on request.

Declaration of competing interest

The authors declare that they have no known competing financial interests or personal relationships that could have appeared to influence the work reported in this paper.

Appendix A. Supplementary data

Supplementary data to this article can be found online at <https://doi.org/10.1016/j.heliyon.2023.e17141>.

References

- [1] M. Rigato, M. Monami, G.P. Fadini, Autologous cell therapy for peripheral arterial disease: systematic Review and meta-analysis of randomized, nonrandomized, and noncontrolled studies, *Circ. Res.* 120 (2017) 1326–1340, <https://doi.org/10.1161/CIRCRESAHA.116.309045>.
- [2] B. De Angelis, P. Gentile, F. Orlandi, I. Bocchini, C. Di Pasquali, A. Agovino, C. Gizzi, F. Patrizi, M.G. Scioli, A. Orlandi, et al., Limb rescue: a new autologous-peripheral blood mononuclear cells technology in critical limb ischemia and chronic ulcers, *Tissue Eng. C Methods* 21 (2015) 423–435, <https://doi.org/10.1089/ten.tec.2014.0245>.
- [3] F. Persiani, A. Paolini, D. Camilli, L. Mascellari, A. Platone, A. Magenta, S. Furgiuele, Peripheral blood mononuclear cells therapy for treatment of lower limb ischemia in diabetic patients: a single-center experience, *Ann. Vasc. Surg.* 53 (2018) 190–196, <https://doi.org/10.1016/j.avsg.2018.05.036>.
- [4] J.M. Grasman, M.J. Zayas, R.L. Page, G.D. Pins, Biomimetic scaffolds for regeneration of volumetric muscle loss in skeletal muscle injuries, *Acta Biomater.* 25 (2015) 2–15, <https://doi.org/10.1016/j.actbio.2015.07.038>.
- [5] M. Fomovsky Leukocyte Purification (EPO 2 602 315 A1).
- [6] E.J. Kim, G.-D. Yeo, C.-M. Pai, I.-K. Kang, Preparation of surface-modified poly(butylene terephthalate) nonwovens and their application as leukocyte removal filters, *J. Biomed. Mater. Res.* 90B (2009) 849–856, <https://doi.org/10.1002/jbm.b.31354>.
- [7] Y. Cao, J. Liu, R. Zhong, Q. Yu, H. Wang, Surface modification of PBT nonwoven fabrics used for blood filtration and their blood compatibility study, *Artif. Cell Blood Substit. Biotechnol.* 40 (2012) 317–325, <https://doi.org/10.3109/10731199.2012.657206>.
- [8] U.G. Longo, M. Loppini, A. Berton, F. Spiezia, N. Maffulli, V. Denaro, Tissue engineered strategies for skeletal muscle injury, *Stem Cell. Int.* 2012 (2012) 1–9, <https://doi.org/10.1155/2012/175038>.
- [9] E.P. Lamparelli, V. Casagrande, D. Pressato, N. Maffulli, G. Della Porta, D. Bellini, Synthesis and characterization of a novel composite scaffold based on hyaluronic Acid and equine type I collagen, *Pharmaceutics* 14 (2022) 1752, <https://doi.org/10.3390/pharmaceutics14091752>.
- [10] E.P. Lamparelli, M.C. Ciardulli, P. Scala, M. Scognamiglio, B. Charlier, P. Di Pietro, V. Izzo, C. Vecchione, N. Maffulli, G. Della Porta, Lipid nano-vesicles for thyroid hormone encapsulation: a comparison between different fabrication technologies, drug loading, and an in vitro delivery to human tendon stem/progenitor cells in 2D and 3D culture, *Int. J. Pharm.* 624 (2022), 122007, <https://doi.org/10.1016/j.ijpharm.2022.122007>.

- [11] S.M. Garcia, S. Tamaki, S. Lee, A. Wong, A. Jose, J. Dreux, G. Kouklis, H. Sbitany, R. Seth, P.D. Knott, et al., High-yield purification, preservation, and serial transplantation of human satellite cells, *Stem Cell Rep.* 10 (2018) 1160–1174, <https://doi.org/10.1016/j.stemcr.2018.01.022>.
- [12] G.W. Charville, T.H. Cheung, B. Yoo, P.J. Santos, G.K. Lee, J.B. Shrager, T.A. Rando, Ex vivo expansion and in vivo self-renewal of human muscle stem cells, *Stem Cell Rep.* 5 (2015) 621–632, <https://doi.org/10.1016/j.stemcr.2015.08.004>.
- [13] D. Montarras, J. Morgan, C. Collins, F. Relaix, S. Zaffran, A. Cumano, T. Partridge, M. Buckingham, Direct isolation of satellite cells for skeletal muscle regeneration, *Science* 309 (2005) 2064–2067, <https://doi.org/10.1126/science.1114758>.
- [14] P. Scala, J. Lovecchio, E.P. Lamparelli, R. Vitolo, V. Giudice, E. Giordano, C. Selleri, L. Rehak, N. Maffulli, G. Della Porta, Myogenic commitment of human stem cells by myoblasts Co-culture: a static vs. a dynamic approach, *Artif. Cell Nanomed. Biotechnol.* 50 (2022) 49–58, <https://doi.org/10.1080/21691401.2022.2039684>.
- [15] M.C. Ciardulli, J. Lovecchio, P. Scala, E.P. Lamparelli, T.P. Dale, V. Giudice, E. Giordano, C. Selleri, N.R. Forsyth, N. Maffulli, et al., 3D biomimetic scaffold for growth factor controlled delivery: an in-vitro study of tenogenic events on wharton's jelly mesenchymal stem cells, *Pharmaceutics* 13 (2021) 1448, <https://doi.org/10.3390/pharmaceutics13091448>.
- [16] M.C. Ciardulli, L. Marino, E.P. Lamparelli, M. Guida, N.R. Forsyth, C. Selleri, G. Della Porta, N. Maffulli, Dose-response tendon-specific markers induction by growth differentiation factor-5 in human bone marrow and umbilical cord mesenchymal stem cells, *Int. J. Math. Stat.* 21 (2020) 5905, <https://doi.org/10.3390/ijms21165905>.
- [17] E.P. Lamparelli, J. Lovecchio, M.C. Ciardulli, V. Giudice, T.P. Dale, C. Selleri, N. Forsyth, E. Giordano, N. Maffulli, G. Della Porta, Chondrogenic commitment of human bone marrow mesenchymal stem cells in a perfused collagen hydrogel functionalized with hTGF- β 1-Releasing PLGA microcarrier, *Pharmaceutics* 13 (2021) 399, <https://doi.org/10.3390/pharmaceutics13030399>.
- [18] M.C. Ciardulli, P. Scala, V. Giudice, A. Santoro, C. Selleri, F. Oliva, N. Maffulli, G. Della Porta, Stem cells from healthy and tendinopathic human tendons: morphology, collagen and cytokines expression and their response to T3 thyroid hormone, *Cells* 11 (2022) 2545, <https://doi.org/10.3390/cells11162545>.
- [19] C. Vater, P. Kasten, M. Stiehler, Culture media for the differentiation of mesenchymal stromal cells, *Acta Biomater.* 7 (2011) 463–477, <https://doi.org/10.1016/j.actbio.2010.07.037>.
- [20] E.P. Lamparelli, M.C. Ciardulli, V. Giudice, P. Scala, R. Vitolo, T.P. Dale, C. Selleri, N.R. Forsyth, N. Maffulli, G. Della Porta, 3D in-vitro cultures of human bone marrow and Wharton's jelly derived mesenchymal stromal cells show high chondrogenic potential, *Front. Bioeng. Biotechnol.* 10 (2022), 986310, <https://doi.org/10.3389/fbioe.2022.986310>.
- [21] Y. Shi, Y. Wang, Q. Li, K. Liu, J. Hou, C. Shao, Y. Wang, Immunoregulatory mechanisms of mesenchymal stem and stromal cells in inflammatory diseases, *Nat. Rev. Nephrol.* 14 (2018) 493–507, <https://doi.org/10.1038/s41581-018-0023-5>.
- [22] S.A. Jacobs, V.D. Roobrouck, C.M. Verfaillie, S.W. Van Gool, Immunological characteristics of human mesenchymal stem cells and multipotent adult progenitor cells, *Immunol. Cell Biol.* 91 (2013) 32–39, <https://doi.org/10.1038/icb.2012.64>.
- [23] T. Winkler, P. von Roth, G. Matziolis, M. Mehta, C. Perka, G.N. Duda, Dose–response relationship of mesenchymal stem cell transplantation and functional regeneration after severe skeletal muscle injury in rats, *Tissue Eng.* 15 (2009) 487–492, <https://doi.org/10.1089/ten.tea.2007.0426>.
- [24] G. Matziolis, T. Winkler, K. Schaser, M. Wiemann, D. Krockner, J. Tuischer, C. Perka, G.N. Duda, Autologous bone marrow-derived cells enhance muscle strength following skeletal muscle crush injury in rats, *Tissue Eng.* 12 (2006) 361–367, <https://doi.org/10.1089/ten.2006.12.361>.
- [25] E. Geijo-Barrientos, C. Pastore-Olmedo, P. De Mingo, M. Blanquer, J. Gómez Espuch, F. Iniesta, N.G. Iniesta, A. García-Hernández, C. Martín-Estefanía, L. Barrios, et al., Intramuscular injection of bone marrow stem cells in amyotrophic lateral sclerosis patients: a randomized clinical trial, *Front. Neurosci.* 14 (2020) 195, <https://doi.org/10.3389/fnins.2020.00195>.
- [26] P.P. Huang, X.F. Yang, S.Z. Li, J.C. Wen, Y. Zhang, Z.C. Han, Randomised comparison of G-CSF-mobilized peripheral blood mononuclear cells versus bone marrow-mononuclear cells for the treatment of patients with lower limb arteriosclerosis obliterans, *Thromb. Haemostasis* 98 (2007) 1335–1342, <https://doi.org/10.1160/TH07-02-0137>.
- [27] J. Moriya, T. Minamino, K. Tateno, N. Shimizu, Y. Kuwabara, Y. Sato, Y. Saito, I. Komuro, Long-term outcome of therapeutic neovascularization using peripheral blood mononuclear cells for limb ischemia, *Circle: Cardiovascular Interventions* 2 (2009) 245–254, <https://doi.org/10.1161/CIRCINTERVENTIONS.108.799361>.
- [28] T. Nevskaya, L. Ananieva, S. Bykovskaia, I. Eremin, E. Karandashov, J. Khrennikov, E. Mach, M. Zaprjagaeva, N. Guseva, E. Nassonov, Autologous progenitor cell implantation as a novel therapeutic intervention for ischaemic digits in systemic sclerosis, *Rheumatology* 48 (2008) 61–64, <https://doi.org/10.1093/rheumatology/ken407>.
- [29] W. Yang, P. Hu, Skeletal muscle regeneration is modulated by inflammation, *Journal of Orthopaedic Translation* 13 (2018) 25–32, <https://doi.org/10.1016/j.jot.2018.01.002>.
- [30] P. Scala, L. Rehak, V. Giudice, E. Ciaglia, A.A. Puca, C. Selleri, G. Della Porta, N. Maffulli, Stem cell and macrophage roles in skeletal muscle regenerative medicine, *Int. J. Math. Stat.* 22 (2021), 10867, <https://doi.org/10.3390/ijms221910867>.
- [31] M. Cheng, M.-H. Nguyen, G. Fantuzzi, T.J. Koh, Endogenous interferon- γ is required for efficient skeletal muscle regeneration, *Am. J. Physiol. Cell Physiol.* 294 (2008) C1183–C1191, <https://doi.org/10.1152/ajpcell.00568.2007>.
- [32] S.-E. Chen, B. Jin, Y.-P. Li, TNF- α regulates myogenesis and muscle regeneration by activating p38 MAPK, *Am. J. Physiol. Cell Physiol.* 292 (2007) C1660–C1671, <https://doi.org/10.1152/ajpcell.00486.2006>.
- [33] J.E. Belizário, C.C. Fontes-Oliveira, J.P. Borges, J.A. Kashiabara, E. Vannier, Skeletal muscle wasting and renewal: a pivotal role of myokine IL-6, *SpringerPlus* 5 (2016) 619, <https://doi.org/10.1186/s40064-016-2197-2>.
- [34] C. Chawewannakorn, M. Tsuchiya, M. Koide, H. Hatakeyama, Y. Tanaka, S. Yoshida, S. Sugawara, Y. Hagiwara, K. Sasaki, M. Kanzaki, Roles of IL-1 α/β in regeneration of cardiotoxin-injured muscle and satellite cell function, *Am. J. Physiol. Regul. Integr. Comp. Physiol.* 315 (2018) R90–R103, <https://doi.org/10.1152/ajpregu.00310.2017>.
- [35] B. Deng, M. Wehling-Henricks, S.A. Villalta, Y. Wang, J.G. Tidball, IL-10 triggers changes in macrophage phenotype that promote muscle growth and regeneration, *J. ICE* 189 (2012) 3669–3680, <https://doi.org/10.4049/jimmunol.1103180>.
- [36] S.A. Villalta, C. Rinaldi, B. Deng, G. Liu, B. Fedor, J.G. Tidball, Interleukin-10 reduces the pathology of mdx muscular dystrophy by deactivating M1 macrophages and modulating macrophage phenotype, *Hum. Mol. Genet.* 20 (2011) 790–805, <https://doi.org/10.1093/hmg/ddq523>.
- [37] E.D. Tsochatzis, J.A. Lopes, M.V. Holland, F. Reniero, H. Emons, C. Guillou, Isolation, characterization and structural elucidation of polybutylene terephthalate cyclic oligomers and purity assessment using a ^1H qNMR method, *Polymers* 11 (2019) 464, <https://doi.org/10.3390/polym11030464>.
- [38] A.P. Dos Santos Pereira, M.H.P. Da Silva, É.P. Lima Júnior, A. Dos Santos Paula, F.J. Tommasini, Processing and characterization of PET composites reinforced with geopolymers concrete waste, *Math. Res.* 20 (2017) 411–420, <https://doi.org/10.1590/1980-5373-mr-2017-0734>.
- [39] M. Ma, L. Niu, J. Ma, J. Ma, T. Jiao, Fabrication and thermal degradation kinetics of PBT/BEO/nano-Sb2O3 composites, *J. Nanomater.* 2020 (2020) 1–10, <https://doi.org/10.1155/2020/6641702>.
- [40] T. Konishi, Y. Miyamoto, Smectic structure and glass transition in poly(butylene terephthalate), *Polym. J.* 42 (2010) 349–353, <https://doi.org/10.1038/pj.2010.5>.
- [41] M.A. Dechet, J.S. Gómez Bonilla, M. Grünwald, K. Popp, J. Rudloff, M. Lang, J. Schmidt, A novel, precipitated polybutylene terephthalate feedstock material for powder bed fusion of polymers (PBF): Material development and initial PBF processability, *Mater. Des.* 197 (2021), 109265, <https://doi.org/10.1016/j.matdes.2020.109265>.
- [42] M. Dominici, K. Le Blanc, I. Mueller, I. Slaper-Cortenbach, F.C. Marini, D.S. Krause, R.J. Deans, A. Keating, D.J. Prockop, E.M. Horwitz, Minimal criteria for defining multipotent mesenchymal stromal cells. The International Society for Cellular Therapy position statement, *Cytotherapy* 8 (2006) 315–317, <https://doi.org/10.1080/14653240600855905>.
- [43] N. Gago-Lopez, O. Awaji, Y. Zhang, C. Ko, A. Nsaïr, D. Liem, A. Stempien-Otero, W.R. MacLellan, THY-1 receptor expression differentiates cardiosphere-derived cells with divergent cardiogenic differentiation potential, *Stem Cell Rep.* 2 (2014) 576–591, <https://doi.org/10.1016/j.stemcr.2014.03.003>.

- [44] F. Relaix, D. Montarras, S. Zaffran, B. Gayraud-Morel, D. Rocancourt, S. Tajbakhsh, A. Mansouri, A. Cumano, M. Buckingham, Pax3 and Pax7 have distinct and overlapping functions in adult muscle progenitor cells, *JCB (J. Cell Biol.)* 172 (2006) 91–102, <https://doi.org/10.1083/jcb.200508044>.
- [45] G. Spaltro, S. Straino, E. Gambini, B. Bassetti, L. Persico, S. Zoli, M. Zanobini, M.C. Capogrossi, R. Spirito, C. Quarti, et al., Characterization of the Pall Celeris system as a point-of-care device for therapeutic angiogenesis, *Cytotherapy* 17 (2015) 1302–1313, <https://doi.org/10.1016/j.jcyt.2015.04.006>.
- [46] S. Rawat, V. Dadhwal, S. Mohanty, Dexamethasone priming enhances stemness and immunomodulatory property of tissue-specific human mesenchymal stem cells, *BMC Dev. Biol.* 21 (2021) 16, <https://doi.org/10.1186/s12861-021-00246-4>.
- [47] D. Liu, B.L. Black, R. Derynck, TGF- β inhibits muscle differentiation through functional repression of myogenic transcription factors by Smad3, *Genes Dev.* 15 (2001) 2950–2966, <https://doi.org/10.1101/gad.925901>.
- [48] N. Osses, E. Brandan, ECM is required for skeletal muscle differentiation independently of muscle regulatory factor expression, *Am. J. Physiol. Cell Physiol.* 282 (2002) C383–C394, <https://doi.org/10.1152/ajpcell.00322.2001>.
- [49] X. Ge, C. McFarlane, A. Vajjala, S. Lokireddy, Z.H. Ng, C.K. Tan, N.S. Tan, W. Wahli, M. Sharma, R. Kambadur, Smad3 signaling is required for satellite cell function and myogenic differentiation of myoblasts, *Cell Res.* 21 (2011) 1591–1604, <https://doi.org/10.1038/cr.2011.72>.
- [50] C. Sassoli, A. Pini, F. Chellini, B. Mazzanti, S. Nistri, D. Nosi, R. Saccardi, F. Quercioli, S. Zecchi-Orlandini, L. Formigli, Bone marrow mesenchymal stromal cells stimulate skeletal myoblast proliferation through the paracrine release of VEGF, *PLoS One* 7 (2012), e37512, <https://doi.org/10.1371/journal.pone.0037512>.
- [51] B.M. Deasy, J.M. Feduska, T.R. Payne, Y. Li, F. Ambrosio, J. Huard, Effect of VEGF on the regenerative capacity of muscle stem cells in dystrophic skeletal muscle, *Mol. Ther.* 17 (2009) 1788–1798, <https://doi.org/10.1038/mt.2009.136>.
- [52] P. Scala, P. Manzo, E.P. Lamparelli, J. Lovecchio, M.C. Ciardulli, V. Giudice, C. Sella, E. Giordano, L. Rehak, N. Maffulli, et al., Peripheral blood mononuclear cells contribute to myogenesis in a 3D bioengineered system of bone marrow mesenchymal stem cells and myoblasts, *Front. Bioeng. Biotechnol.* 10 (2023), 1075715, <https://doi.org/10.3389/fbioe.2022.1075715>.
- [53] R. Longo, M. Catauro, A. Sorrentino, L. Guadagno, Thermal and mechanical characterization of complex electrospun systems based on polycaprolactone and gelatin, *J. Therm. Anal. Calorim.* 147 (2022) 5391–5399, <https://doi.org/10.1007/s10973-022-11225-7>.
- [54] K. Havlíček, L. Svobodová, T. Bakalova, T. Lederer, Influence of electrospinning methods on characteristics of polyvinyl butyral and polyurethane nanofibres essential for biological applications, *Mater. Des.* 194 (2020), 108898, <https://doi.org/10.1016/j.matdes.2020.108898>.
- [55] P. Manzo, P. Scala, V. Giudice, M. Gorrese, A. Bertolini, D. Morini, F. D'Alto, R. Pepe, A. Pedicini, B. Izzo, et al., c-Kit M541L variant is related to ineffective hemopoiesis predisposing to clonal evolution in 3D in vitro biomimetic co-culture model of bone marrow niche, *Heliyon* 8 (2022), e11998, <https://doi.org/10.1016/j.heliyon.2022.e11998>.
- [56] J. Hellemans, G. Mortier, A. De Paepe, F. Speleman, J. Vandesompele, qBase 277 relative quantification framework and software for management and automated 278 analysis of real-time quantitative PCR, *Genome Biol.* 8 (2007) R19, <https://doi.org/10.1186/gb-2007-8-2-r19>.
- [57] de Winter, J.C.F. Using the Student's T-Test with Extremely Small Sample Sizes. 10.7275/E4R6-DJ05.